The distance and internal composition of the neutron star in EXO 0748-676 with XMM-Newton

Zhang, Guobao; Mendez, Mariano; Jonker, Peter; Hiemstra, Beike

Published in:
Monthly Notices of the Royal Astronomical Society

DOI:
10.1111/j.1365-2966.2011.18443.x

Publication date:
2011

Monthly Notices
of the
ROYAL ASTRONOMICAL SOCIETY

Mon. Not. R. Astron. Soc. **414,** 1077–1081 (2011) doi:10.1111/j.1365-2966.2011.18443.x

The distance and internal composition of the neutron star in EXO 0748−676 with *XMM–Newton*

Guobao Zhang,[1⋆] Mariano Méndez,[1] Peter Jonker[2,3,4] and Beike Hiemstra[1]

[1] *Kapteyn Astronomical Institute, University of Groningen, PO Box 800, 9700 AV Groningen, the Netherlands*
[2] *SRON, Netherlands Institute for Space Research, Sorbonnelaan 2, 3584 CA Utrecht, the Netherlands*
[3] *Harvard–Smithsonian Center for Astrophysics, 60 Garden Street, Cambridge, MA 02138, USA*
[4] *Department of Astrophysics, IMAPP, Radboud University Nijmegen, PO Box 9010, 6500 GL Nijmegen, the Netherlands*

Accepted 2011 January 28. Received 2011 January 25; in original form 2010 June 20

ABSTRACT

Recently, the neutron star X-ray binary EXO 0748−676 underwent a transition to quiescence. We analysed an *XMM–Newton* observation of this source in quiescence, where we fitted the spectrum with two different neutron star atmosphere models. From the fits we constrained the allowed parameter space in the mass–radius diagram for this source for an assumed range of distances to the system. Comparing the results with different neutron star equations of state, we constrained the distance to EXO 0748−676. We found that strange quark matter equation of state is consistent with the mass and radius from our fits only if EXO 0748−676 is at a distance of less than 5 kpc, whereas the normal neutron star equation of state is consistent with our best-fitting mass and radius if the distance is ∼7 kpc, as deduced from properties of the X-ray bursts.

Key words: dense matter – equation of state – stars: individual: EXO 0748−676 – stars: neutron – X-rays: binaries.

1 INTRODUCTION

The low-mass X-ray binary (LMXB) EXO 0748−676 was discovered as a transient source with the European X-ray Observatory Satellite (*EXOSAT*) in 1985 (Parmar et al. 1986). The source exhibits simultaneous X-ray and optical eclipses from which an orbital period of 3.82 h was deduced (Crampton et al. 1986). EXO 0748−676 also shows irregular X-ray dipping activity (Parmar et al. 1986), and type I X-ray bursts (Gottwald et al. 1986). Burst oscillations in EXO 0748−676 were first reported by Villarreal & Strohmayer (2004) at 45 Hz in the average Fourier power spectrum of 38 type I X-ray bursts; the 45-Hz signal was then interpreted as the spin frequency of the neutron star (NS). Recently, Galloway, Chakrabarty & Lin (2009) detected millisecond oscillations in the rising phase of two type I X-ray bursts in EXO 0748−676 at a frequency of 552 Hz. They concluded that the spin frequency of EXO 0748−676 is close to 522 Hz, rather than 45 Hz as suggested by Villarreal & Strohmayer (2004). The 45-Hz oscillation may arise in the boundary layer between the disc and the NS (Balman 2009) or it could be a statistical fluctuation (Galloway et al. 2009). Cottam, Paerels & Méndez (2002) reported a measurement of the gravitational redshift from iron and oxygen X-ray absorption lines arising from the atmosphere of the NS in EXO 0748−676 during type I X-ray bursts, but subsequent observations failed to confirm these features (Cottam et al. 2008). Based on the gravitational redshift, Özel (2006) suggested that the mass, radius and distance of EXO 0748−676 are $2.10 \pm 0.28\,M_{\odot}$, 13.8 ± 1.8 km and 9.2 ± 1.0 kpc, respectively, which would rule out many NS equations of state (EOSs).

Measuring the distance to LMXBs is difficult, except in the case of sources in globular clusters. A way to get the distance is using type I X-ray bursts. The peak flux for some very bright bursts can reach the Eddington luminosity at the surface of the NS. From a strong X-ray burst, Wolff et at. (2005) derived a distance to EXO 0748−676 of 7.7 kpc for a helium burst, and 5.9 kpc for a hydrogen burst. Galloway et al. (2008a) analysed several type I X-ray bursts from EXO 0748−676 and estimated a distance of 7.4 kpc, different from the value of 9.2 kpc reported by Özel (2006). Taking into account the touchdown flux and the high binary inclination of EXO 0748−676, recently Galloway, Özel & Psaltis (2008b) gave a distance of 7.1 ± 1.2 kpc.

Another way to get the distance to an LMXB is through observations of quiescent X-ray emission from the NS surface. During the quiescent state, X-ray emission originates from the atmosphere of the NS. By fitting the X-ray spectrum with hydrogen atmosphere models, one can estimate the mass, radius and distance of the NS. Recently, the NS X-ray transient EXO 0748−676 underwent a transition into quiescence (Bassa et al. 2009; Degenaar et al. 2009). Using *Chandra* data, Degenaar et al. (2009) found a distance of $3.4^{+1.4}_{-0.7}$ kpc to EXO 0748−676 for canonical NS mass and radius values of $M_{\rm NS} = 1.4\,M_{\odot}$ and $R_{\rm NS} = 10$ km, respectively. The

⋆E-mail: zhang@astro.rug.nl

fitted distance is lower than that obtained from type I X-ray bursts (Galloway et al. 2008a,b).

In this paper, we report on the distance to EXO 0748−676 that deduced from *XMM–Newton* data. We use two different NS atmosphere models to fit the X-ray spectrum, and compare the results of the spectral fitting with different NS EOSs. In the next section, we describe the observation and data analysis. We show the fitting results in Section 3, and we discuss our findings in Section 4.

2 OBSERVATIONS AND DATA ANALYSIS

EXO 0748−676 was observed with the European Photon Imaging Camera (EPIC) using the PN and Metal-Oxide-Silicon (MOS) detectors onboard the *XMM–Newton* on 2008 November 6 at 08:30:03 UTC (obsID 0560180701). The PN and the two MOS cameras were operated in full-window mode. We reduced the *XMM–Newton* Observation Data Files (ODF) using version 8.0.0 of the Science Analysis Software (SAS). We used the EPPROC and EMPROC tasks to extract the event files for the PN and the two MOS cameras, respectively. Source light curves and spectra were extracted in the 0.2–12.0 keV band using a circular extraction region with a radius of 30 arcsec centred on the position of the source. Background light curves and spectra were extracted from a circular source-free region of 35 arcsec on the same CCD. We applied standard filtering and examined the light curves for background flares. No flares were present and we used the whole exposure for our analysis. The exposure time for the PN camera was 24.2 ks, and for each MOS camera was 29.03 ks. The source count rate was 0.496 ± 0.005 counts s^{-1} for PN, and 0.135 ± 0.002 and 0.127 ± 0.002 counts s^{-1} for MOS1 and MOS2, respectively. We checked the filtered event files for photon pile-up by running the task EPATPLOT. No pile-up was apparent in the PN, MOS1 and MOS2 data. Photon redistribution matrices and ancillary files were created using the SAS tools RMFGEN and ARFGEN, respectively. We rebinned the source spectra using the tool PHARBN (Guainazzi, private communication), such that the number of bins per resolution element of the PN and MOS spectra was 3 and the minimum number of counts per channel was 20.

We fitted the PN and MOS spectra simultaneously in the 0.5–10.0 keV range with XSPEC 12.50 (Arnaud 1996), using either of two NS hydrogen atmosphere models: NSAGRAV (Zavlin, Pavlov & Shibanov 1996) or NSATMOS (Heinke et al. 2006). The NSAGRAV model provides the spectra emitted from a non-magnetic hydrogen atmosphere of a NS with surface gravitational acceleration, g, ranging from 10^{13} to 10^{15} cm s^{-2}. This model uses the mass ($M_{\rm NS}$) and radius ($R_{\rm NS}$) of the NS and the unredshifted effective temperature of the surface of the star ($kT_{\rm eff}$) as parameters. The normalization of the model is defined as $1/D^2$, where D is the distance to the source in parsec. The second model that we used, NSATMOS, includes a range of surface gravities and effective temperatures, and incorporates thermal electron conduction and self-irradiation by photons from the compact object. This model assumes negligible magnetic fields (less than 10^9 G) and a pure hydrogen atmosphere. NSATMOS parameters are $M_{\rm NS}$, $R_{\rm NS}$, log$T_{\rm eff}$ (the same as for NSAGRAV), distance in kiloparsec and a separate normalization K, which corresponds to the fraction of the NS surface that is emitting. We fixed K to be 1 in all our fits with NSATMOS.

We included the effect of interstellar absorption using 'phabs' assuming cross-sections of Balucinska-Church & McCammon (1992) and solar abundances from Anders & Grevesse (1989), and we let $N_{\rm H}$, the column density along the line of sight, free to vary during the fitting. In order to account for differences in effective area between the different cameras, we introduced a multiplicative factor in our model. First, this factor was fixed to unity for PN and left free for MOS1 and MOS2. Subsequently, we set the scaling factor to unity for MOS1 and MOS2, respectively, and left the factor free for the other cameras. We found that fixing the scaling factor for different cameras gives similar best-fitting results. Therefore, in the rest of the paper we fixed the factor to 1 for PN and left it free to vary for the other cameras. None of the atmosphere models alone fitted the spectrum above ∼2–3 keV properly. Adding a power-law component improved the fits significantly, however, all parameters were less constrained than when we fitted the data with the NS atmosphere model only. We first fixed the power-law index to 0.5, 1.0 and 1.5 to get better constraints on the parameters of the NS atmosphere model (see Degenaar et al. 2009). We initially fixed the distance to the NS at 7.1 kpc, which is the value inferred from the touchdown flux of Galloway et al. (2008b).

3 RESULTS

3.1 Results from the spectral fits

Fig. 1 shows the *XMM–Newton* spectra of EXO 0748−676 fitted with the model 'phabs (NSATMOS + powerlaw)'. The power-law index was fixed at 1.0 in this case. The best fit of this model gives $N_{\rm H} = 6.1 \pm 1.5 \times 10^{20}$ cm^{-2}, NS mass $M_{\rm NS} = 1.55 \pm 0.12\,{\rm M}_{\odot}$, NS radius $R_{\rm NS} = 16.0^{+0.7}_{-1.3}$ km and effective temperature $\log T_{\rm eff} = 6.20 \pm 0.02$ (in K). According to the same formula $T^{\infty}_{\rm eff} = T_{\rm eff}\sqrt{1-(2GM_{\rm NS})/(R_{\rm NS}c^2)}$ used by Degenaar et al. (2009), we converted $T_{\rm eff}$ to the effective temperature as seen by an observer at infinity, $T^{\infty}_{\rm eff} = 114 \pm 4$ eV. In the formula, G is the gravitational constant and c is the speed of light. The model predicts a 0.5–10 keV unabsorbed X-ray flux $F_{\rm X} = 1.13 \pm 0.06 \times 10^{-12}$ erg cm^{-2} s^{-1}. The flux of the power-law component in the same energy band is $F_{\rm pow} = 1.11 \pm 0.15 \times 10^{-13}$ erg cm^{-2} s^{-1}, which corresponds to ∼10 per cent of the total unabsorbed flux. The reduced χ^2 is 0.977 for 219 degrees of freedom. The best-fitting results of the models NSAGRAV and NSATMOS for the three different power-law indexes are given in Table 1. Errors are given at the 90 per cent confidence level for one-fit parameter.

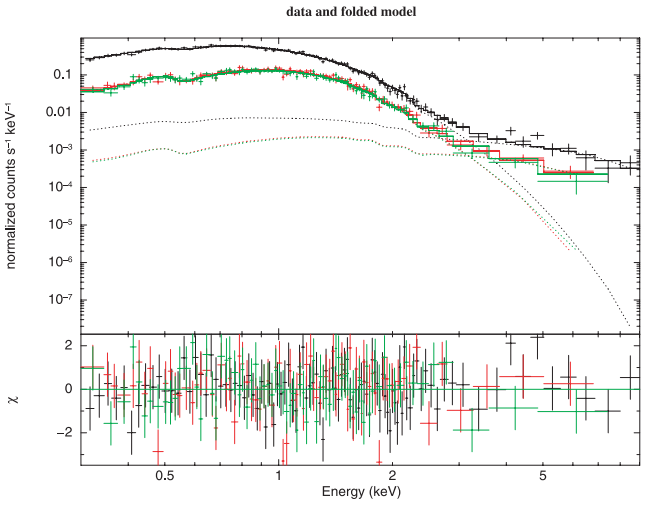

Figure 1. *XMM–Newton* PN (black), MOS1 (red) and MOS2 (green) spectrum of EXO 0748−676 in the 0.5–10.0 keV energy band. The spectrum was fitted with a NS hydrogen atmosphere model (NSATMOS) and a power-law model with Γ fixed to 1. The lower panel shows the residuals to the best-fitting model in unit of σ.

Table 1. Best-fitting parameters of NS atmosphere models fit to the *XMM–Newton* data of EXO 0748−676.

Model	$N_{\rm H}$ (10^{20} cm^{-2})	$T_{\rm eff}^{\infty}$ (eV)	$M_{\rm NS}$ ($M_{\odot}$)	$R_{\rm NS}$ (km)	Γ	$F_{\rm pow}$ (10^{-13} erg cm^{-2} s^{-1})	$F_{\rm X}$ (10^{-12} erg cm^{-2} s^{-1})	χ^2/d.o.f.
NSAGRAV	5.6 ± 1.8	113^{+14}_{-8}	1.55 ± 0.18	15.2 ± 1.8	0.5	1.15 ± 0.21	1.18 ± 0.15	0.986/219
NSATMOS	5.4 ± 1.5	113 ± 4	1.29 ± 0.20	$16.1^{+0.9}_{-1.2}$	0.5	1.17 ± 0.20	1.23 ± 0.16	0.985/219
NSAGRAV	$6.2^{+1.3}_{-1.8}$	114^{+24}_{-3}	1.62 ± 0.11	$15.8^{+0.25}_{-3.5}$	1.0	1.10 ± 0.15	1.14 ± 0.13	0.977/219
NSATMOS	6.1 ± 1.5	114 ± 4	1.55 ± 0.12	$16.0^{+0.7}_{-1.3}$	1.0	1.11 ± 0.15	1.13 ± 0.06	0.977/219
NSAGRAV	6.7 ± 1.5	110 ± 8	1.71 ± 0.30	16.5 ± 0.5	1.5	1.00 ± 0.19	1.01 ± 0.15	0.987/219
NSATMOS	6.7 ± 1.4	110 ± 5	1.77 ± 0.45	$16.6^{+1.8}_{-7.5}$	1.5	1.03 ± 0.22	1.03 ± 0.10	0.985/219

Note. $N_{\rm H}$ is the equivalent hydrogen column density, $T_{\rm eff}^{\infty}$ the effective temperature of the NS surface as seen at infinity and $M_{\rm NS}$ and $R_{\rm NS}$ are the mass and radius of the NS, respectively. $F_{\rm pow}$ is the unabsorbed flux of the power-law component in the 0.5–10 keV energy band, and $F_{\rm X}$ is the total unabsorbed X-ray flux in the same energy band. The last column gives the reduced χ^2 for 219 degrees of freedom. The quoted errors represent the 90 per cent confidence levels. The power-law index (Γ) was kept fixed at the value given in the table during the fits.

We note from Table 1 that both atmosphere models, regardless of the value of Γ, yield a good fit with similar χ^2, and the best-fitting parameters are consistent with being the same for the three values of Γ. In the rest of the analysis, we used a power-law index fixed to 1. The NSATMOS model is more accurate in constraining $T_{\rm eff}$ than the NSAGRAV model.

3.2 Equation of state

Fitting the quiescence *XMM–Newton* spectrum of EXO 0748−676 with two different atmosphere models and comparing the results allows us to test the reliability and accuracy of both models. From the fits we find a mass and radius of the NS at a specified distance, and by comparing the inferred mass and radius with the different NS EOSs we can give upper limits to the source distance for the different EOS models.

We used the STEPPAR command in XSPEC to vary the mass, radius and distance parameters simultaneously, allowing other parameters to be free to find the best fit at each step. For the mass we go from 0.5 to 2.5 $M_{\odot}$ with steps of 0.1 $M_{\odot}$, and for the distance we go from 5 to 10 kpc with steps of 0.25 kpc. The minimum and maximum radius allowed by these models are 5.0 and 25.0 km, respectively. In Fig. 2 we show the contour plots obtained from the STEPPAR procedure for the NSATMOS model. Each plot is for a different distance, ranging from 5 to 10 kpc. The contour lines (red) are for the confidence levels of 90 (solid) and 99 per cent (dashed). Further, in Fig. 2 we show different NS EOSs (black) taken from Lattimer & Prakash (2007). We did the same analysis for the NSAGRAV model. Both NSATMOS and NSAGRAV models give consistent results, in accordance with the findings of Webb & Barret (2007).

Using optical data from the Very Large Telescope (VLT), Muñoz-Darias et al. (2009) provided the first dynamical constraint on the mass of the NS in LMXB EXO 0748−676. The mass range of the NS that they derived is $1 \leq M_{\rm NS} \leq 2.4\,M_{\odot}$. Subsequently, Bassa et al. (2009) analysed optical spectra of EXO 0748−676 when the source was in quiescence, and they found a lower limit to the NS mass of $M_{\rm NS} \geq 1.27\,M_{\odot}$. We show the upper limit (pink/dotted) reported by Muñoz-Darias et al. (2009) and the lower limit (green/dashed) reported by Bassa et al. (2009).

The internal composition of the cores of NSs is currently poorly understood. In order to test the EOS and identify the upper limit to the source distance, we here assume three typical EOS models with different core composition: normal nucleonic matter (AP3), boson condensates matter (MS1) and strange quark matter (SQM1). By varying the source distance from 5 to 10 kpc, the contour lines for the fitted model move on the NS mass–radius diagram. We can estimate the probability of the distance for each EOS when the contour lines pass through the EOS curves. Note that as the distance increases (see Fig. 2), the allowed area of the model moves from the bottom left to the top right in the plot. The results using NSAGRAV are similar to those shown in Fig. 2. For a given distance we found that not all the EOSs are consistent with the two NS atmosphere models that we used. The upper limits on the distance to EXO 0748−676 for different EOS are shown in Table 2.

If the NS in EXO 0748−676 follows the EOS model 'AP3', the probability that the source has a distance of 10.0 kpc is 1×10^{-4} and 1×10^{-6} for NSAGRAV and NSATMOS, respectively. If we want to get a probability for the distance larger than 1×10^{-2} (99 per cent confidence), the distance for NSAGRAV and NSATMOS should be smaller than 8.9 and 8.5 kpc, respectively. The distance at 90 per cent confidence for NSAGRAV and NSATMOS is less than 8.3 and 8.2 kpc, respectively. Both models are consistent with the distance of 7.1 kpc given by type I X-ray bursts (Galloway et al. 2008b).

For the EOS model 'MS1', the probability that EXO 0748−676 is at a distance of 10 kpc is 10^{-5} and 10^{-6} for NSAGRAV and NSATMOS, respectively. For both models, respectively, the distance at 99 per cent confidence level is less than 7.3 and 7.1 kpc, and the distance at 90 per cent confidence level is less than 6.9 and 6.8 kpc, which are smaller than the distance of 7.1 kpc deduced from the bursts.

For the EOS model 'SQM1', the distance at 99 per cent confidence level is less than 5.2 kpc, and the distance at 90 per cent confidence level is less than 5.0 kpc for both atmosphere models. The 'SQM1' model is rejected at a 99 per cent confidence level for this NS, unless the source is closer than 5.2 kpc.

4 DISCUSSION

We analysed an *XMM–Newton* observation of the NS EXO 0748−676 in the quiescent state. The unabsorbed X-ray flux in the 0.5–10.0 keV energy band was $(1.13 \pm 0.06) \times 10^{-12}$ erg cm^{-2} s^{-1}. We found that the non-thermal (power-law) component only contributes $\sim 10 \pm 2$ per cent of the 0.5–10 keV X-ray flux, which is lower than what Degenaar et al. (2009) found from the *Chandra* data ($F_{\rm pow}$ was ∼16–17 per cent of the 0.5–10 keV X-ray flux from the fit with $\Gamma = 1$) about a month earlier than our observation. The 0.5–10 keV unabsorbed flux and the effective temperature in our *XMM–Newton* observations are consistent with the value obtained from the *Chandra* observation, and also with the

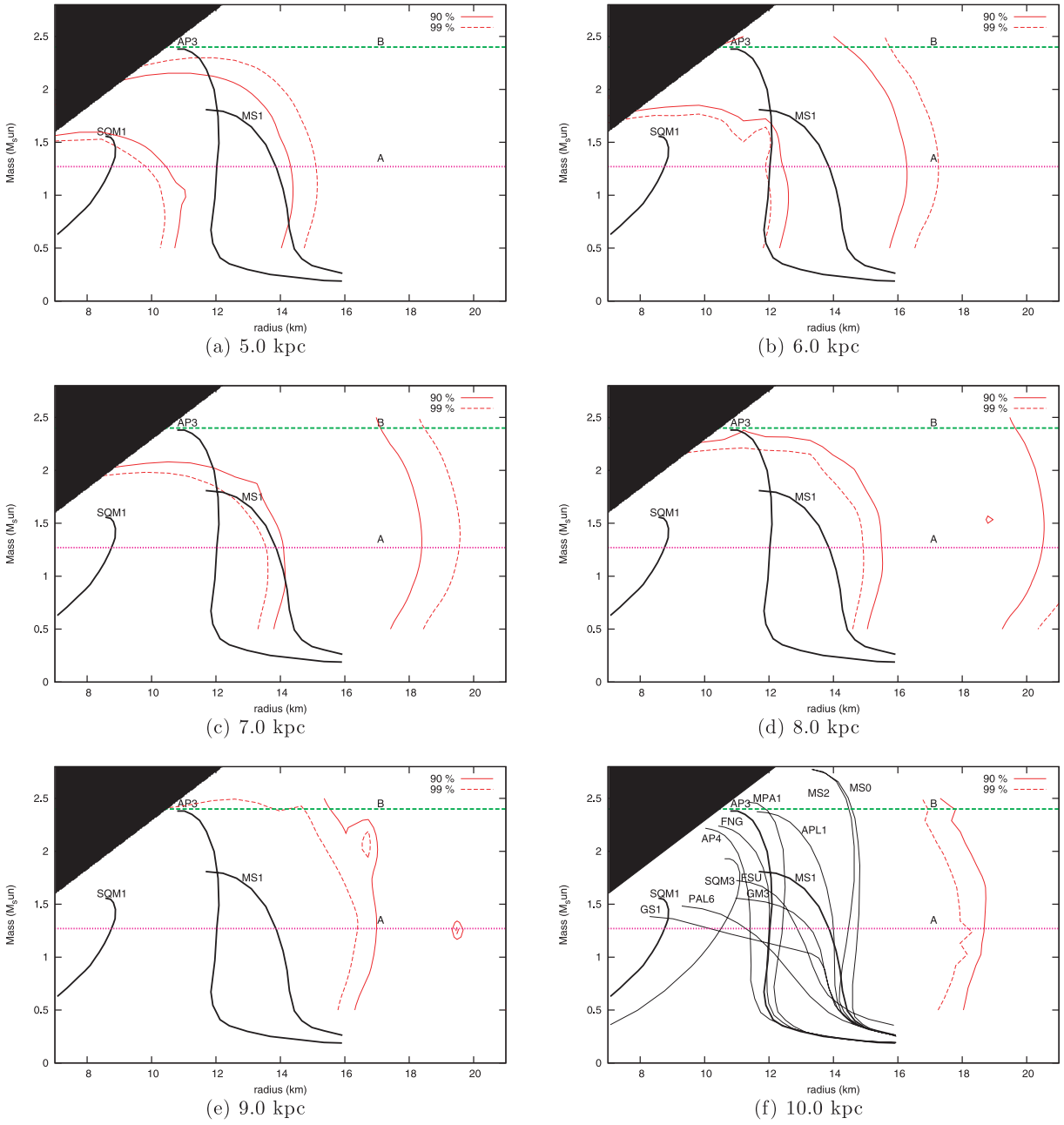

Figure 2. Contour plots showing the results of modelling the NS in EXO 0748−676 with the XSPEC model NSATMOS and a power law. The power-law index is fixed to 1. The plots show two confidence levels in the mass–radius diagram obtained from our fit; the contour lines (red) are for the confidence levels of 90 and 99 per cent, respectively. The pink line 'A' shows the lower limit of the NS mass given by Bassa et al. (2009), and the green line 'B' shows the upper limit given by Muñoz-Darias et al. (2009).

Table 2. Upper limits on the distance to EXO 0748−676 for different EOS models.

Model	AP3 90 per cent	AP3 99 per cent	MS1 90 per cent	MS1 99 per cent	SQM1 90 per cent	SQM1 99 per cent
NSAGRAV	$D < 8.3$ kpc	$D < 8.9$ kpc	$D < 6.9$ kpc	$D < 7.3$ kpc	$D < 5.0$ kpc	$D < 5.2$ kpc
NSATMOS	$D < 8.2$ kpc	$D < 8.5$ kpc	$D < 6.8$ kpc	$D < 7.1$ kpc	$D < 5.0$ kpc	$D < 5.2$ kpc

Note. The 90 and 99 per cent confidence levels upper limit to the distance to EXO 0748−676 for the two NS atmosphere models NSAGRAV and NSATMOS for the EOS models: 'AP3', 'MS1' and 'SQM1'. The distance is in kpc.

value of the *Swift* observation closest in time to our *XMM–Newton* observation (Degenaar et al. 2009). However, our best-fitting $N_{\rm H}$ value is a factor of ∼2 lower than the one from the *Chandra* observation. If we fix $N_{\rm H}$ in our fits to the value of Degenaar et al. (2009), the 0.5–10 keV flux does not change significantly.

In their table 1, Degenaar et al. (2009) presented the fitting results of *Chandra* data using the NSATMOS model for different distance, similar to what we do here. From their results when Γ fixed at 1, we find that their best-fitting NS mass and radius are always consistent with our 90 per cent confidence contour lines.

Since the X-ray spectrum in the quiescent state is dominated by thermal emission originating from the NS surface, our fits to the data using NS atmosphere models allow us to constrain the mass and radius of the NS EXO 0748−676. Using two different NS atmosphere models, NSAGRAV and NSATMOS, we found consistent results, and we could set good constraints on the NS radius. Even taking into account the lower limit (Bassa et al. 2009) and upper limit (Muñoz-Darias et al. 2009) to the NS mass and our best-fitting $\Delta\chi^2$ contour, a large area on the mass–radius diagram is allowed by the data, and many EOSs are still possible (see Fig. 2). In order to constrain the allowed space of mass and radius at a specified distance, we choose three typical NS EOS models: 'AP3', 'MS1' and 'SQM1'. We found that the smaller the distance to the NS the more EOSs are consistent with the data.

For a specific EOS, we took the upper limit to the distance as the value of the distance where the 99 per cent confidence contour just intersects the curve of that EOS. We found that the upper limits to the distance derived from the NSAGRAV model are slightly higher than those for the NSATMOS model. The EOS model 'MS1' can be just satisfied at a distance of 7.1 kpc. If we assume that the NS in EXO 0748−676 is a normal NS, for the EOS 'AP3' the source should be closer than 8.9 kpc for the NSAGRAV model, or 8.5 kpc for the NSATMOS model. Both the 'MS1' and 'AP3' EOS are fully consistent with the distance of 7.1 kpc deduced from the X-ray bursts (Wolff et at. 2005; Galloway et al. 2008b). For larger distances more EOSs are ruled out. The EOS 'SQM1' is rejected by the NS atmosphere model fits for a distance of 7.1 kpc. We note, however, that the NS atmosphere models may not be appropriate for 'bare' quark matter stars.

ACKNOWLEDGMENTS

This work is based on the observations obtained from *XMM–Newton*. We acknowledge an anonymous referee for useful comments. PJ acknowledges support from a VIDI grant from the Netherlands Organisation for Scientific Research.

REFERENCES

Anders E., Grevesse N., 1989, Geochimica Cosmochimica Acta, 53, 197
Arnaud K. A., 1996, in Jacoby G., Barnes J., eds, ASP Conf. Ser. Vol. 101, Astronomical Data Analysis Software and Systems V. Astron. Soc. Pac., San Francisco, p. 17
Balman S., 2009, Astron. Telegram, 2097
Balucinska-Church M., McCammon D., 1992, ApJ, 400, 699
Bassa C. G., Jonker P. G., Steeghs D., Torres M. A. P., 2009, MNRAS, 399, 2055
Cottam J., Paerels F., Méndez M., 2002, Nat, 420, 51
Cottam J., Paerels F., Méndez M., Boirin L., Lewin W. H. G., Kuulkers E., Miller J. M., 2008, ApJ, 672, 504
Crampton D., Stauffer J., Hutchings J. B., Cowley A. P., Ianna P., 1986, ApJ, 306, 599
Degenaar N. et al., 2009, MNRAS, 396, L26
Galloway D. K., Muno M. P., Hartman J. M., Savov P., Psaltis D., Chakrabarty D., 2008a, ApJS, 179, 360
Galloway D. K., Özel F., Psaltis D., 2008b, MNRAS, 387, 268
Galloway D. K., Chakrabarty D., Lin R., 2009, Astron. Telegram, 2094
Gottwald M., Haberl F., Parmar A. N., White N. E., 1986, ApJ, 308, 213
Heinke C. O., Rybicki G. B., Narayan R., Grindlay J. E., 2006, ApJ, 644, 1090
Lattimer J. M., Prakash M., 2007, Phys. Rep., 442, 109
Muñoz-Darias T., Casares J., O(tm)Brien K., Steeghs D., Mart'nez-Pais I. G., Cornelisse R., Charles P. A., 2009, MNRAS, 394, L136
Özel F., 2006, Nat, 441, 1115
Parmar A. N., White N. E., Giommi P., Gottwald M., 1986, ApJ, 308, 199
Villarreal A. R., Strohmayer T. E., 2004, ApJ, 614, L121
Webb N. A., Barret D., 2007, ApJ, 671, 727
Wolff M. T., Becker P. A., Ray P. S., Wood K. S., 2005, ApJ, 632, 1099
Zavlin V. E., Pavlov G. G., Shibanov Y. A., 1996, A&A, 315, 141

This paper has been typeset from a TEX/LATEX file prepared by the author.